Calculated Valence-Band Densities of States and Photoemission Spectra of Diamond and Zinc-Blende Semiconductors*

J. Chelikowsky,† D. J. Chadi, and Marvin L. Cohen
Department of Physics and Inorganic Materials Research Division, Lawrence Berkeley Laboratory, University of California, Berkeley, California 94720
(Received 24 April 1973)

Density-of-states calculations are presented based on band structures computed using the empirical pseudopotential method. Data from recent measurements of x-ray photoemission spectra and ultraviolet photoemission spectra are used to obtain the theoretical parameters. It was necessary to include a nonlocal pseudopotential to obtain consistency with experiment. Results for the density of states, including critical-point assignments and band structures, are given for Si, Ge, GaAs, InSb, GaP, ZnSe, and CdTe.

I. INTRODUCTION

With the advent of high-resolution photoemission spectroscopy, i.e., x-ray photoemission spectroscopy (XPS) and ultraviolet photoemission spectroscopy (UPS), detailed information is now available[1-3] about the lowest-lying valence bands in semiconductors. In this paper we identify the structure in those spectra and associate it with structure in the valence-band density of states. To do this we have calculated the band structures and density of states for Si, Ge, GaAs, GaP, InSb, ZnSe, and CdTe using the empirical pseudopotential method (EPM).[4,5]

The EPM uses experimental data to fix the form factors of the crystalline potential. In the past, reflectivity data were the main source of experimental input. It was found that a completely local potential was sufficient to explain most of the reflectivity data. On purely theoretical grounds the pseudopotential should be nonlocal and energy dependent, but local approximations suffice for a limited energy range. This is the situation for the reflectivity case where the predominant structure results from transitions between the top valence and bottom conduction bands. When we extend the early calculations to lower energies into the valence bands, comparisons with XPS and UPS data show discrepancies. In addition, reflectivity assignments fit direct transitions. When XPS or UPS data are used, it is possible to fix indirect splittings. It was found that even regions of the second-highest valence bands were in disagreement with experiment. A nonlocal pseudopotential scheme completely removes the discrepancies above. In this paper we take the simplest approach to get the lowest-order corrections by allowing the electron mass to vary, i.e., $m \to m^*$. A more traditional (and theoretically pleasing) approach[4] would be to include a specific nonlocal potential (e.g., for d waves). We have done such calculations for the density of states, and we find results which are similar to those obtained using m^*. We therefore have chosen the former scheme because it is simple.

We begin by calculating the density of states with a local potential and then fit the nonlocal parameter, i.e., m^* and the form factors of the potential, by comparing the density of states with XPS and UPS data. One of the most striking features of the XPS and UPS spectra is that they both mimic the valence-band density of states. In addition, the agreement between the two (XPS and UPS) is excellent. *Considering that the bulk penetration of electrons is different in the two cases this adds support to the idea that both XPS and UPS measure bulk properties.*

After the density-of-states fits are obtained (reflectivity data are also used as a constraint), a critical-point (cp) analysis is done. The sharp structure is identified with the M_0, M_1, M_2, M_3 cp's[4] in the energy-band structure. The band structure itself is given for each crystal studied.

The over-all agreement is good and the major discrepancies between experiment and the local EPM calculations have been removed especially for the highest valence bands. The lowest band is the least reliable; this stems partially from the approximate manner in which we have included nonlocal effects.

In the text, comparison is made between the present calculation using the nonlocal potential, experimental results, and the original calculations using the EPM by Cohen and Bergstresser[5] (CB). More recent EPM calculations since CB have been done which give better agreement with experimental reflectivity spectra. However, in these calculations again very little attention is given to fitting the valence-band densities of states. Despite this, the adjustment to fit optical data sometimes yielded a band structure which gave density-of-states spectra closer to the XPS value. We have not, however, included these results here, as it is more straightforward and simpler to use the CB values since this reference contains all the crystals of interest and the form factors are not too different from the more recent work.

TABLE I. Form factors (in Ry), effective-mass parameter, and lattice constants (in Å).

	$V^S(3)$	$V^S(8)$	$V^S(11)$	$V^A(3)$	$V^A(4)$	$V^A(11)$	m/m^*	a
Si	−0.211	0.040	0.080	•••	•••	•••	•••	5.43
Ge	−0.269	0.038	0.035	•••	•••	•••	1.089	5.65
GaAs	−0.252	0.000	0.080	0.068	0.066	0.012	1.138	5.64
GaP	−0.249	0.017	0.083	0.081	0.055	0.003	1.075	5.45
ZnSe	−0.261	−0.011	0.113	0.151	0.130	0.016	1.291	5.65
InSb	−0.250	0.010	0.044	0.049	0.038	0.010	1.192	6.47
CdTe	−0.245	−0.015	0.073	0.089	0.084	0.006	1.228	6.48

II. METHODS OF CALCULATION

The EPM involves adjusting pseudopotential form factors to achieve good agreement with the experimental results. These form factors are then used to calculate the electronic energy bands on a fine mesh of points throughout the Brillouin zone.[4]

In applying the EPM to obtain the electronic band structures, we have used the pseudopotential Hamiltonian

$$H = -(\hbar^2/2m^*)\nabla^2 + V(\vec{r}), \tag{1}$$

where m^* is an effective mass and $V(\vec{r})$ is a weak pseudopotential which is taken to be a superposition of spherical atomic pseudopotentials.

The potential $V(\vec{r})$ is then expanded in reciprocal lattice vectors, and for convenience expressed in terms of a symmetric and antisymmetric part:

$$V(\vec{r}) = \sum_{\vec{G}} [V^S(G)\cos\vec{G}\cdot\vec{\tau} + iV^A(G)\sin\vec{G}\cdot\vec{\tau}]e^{(-i\vec{G}\cdot\vec{r})}, \tag{2}$$

where $\vec{\tau} = \frac{1}{8}a(1,1,1)$, a being the lattice constant. [For diamond structure compounds, the antisym-

TABLE II. Energies (in eV) of characteristic features in the valence band of Si (measured relative to the top of the valence band).

Si	Theory (Ref. 5)	Experiment UPS (Refs. 3, 14)	Experiment XPS (Refs. 1, 2, 13)
L_3'	−1.1	•••	•••
X_4	−2.8	•••	−2.5±0.3
W_2	−4.0	•••	−3.9±0.2
$\Sigma_1^{\min}$	−4.5	−4.7±0.2	−4.7±0.3
L_1	−7.2	−6.4±0.4	−6.8±0.2
W_1	−8.1	•••	−8.1±0.3
Γ_2'	−10.2	•••	−9.3±0.4
Γ_1	−12.6	−12.4±0.6	−12.5±0.6

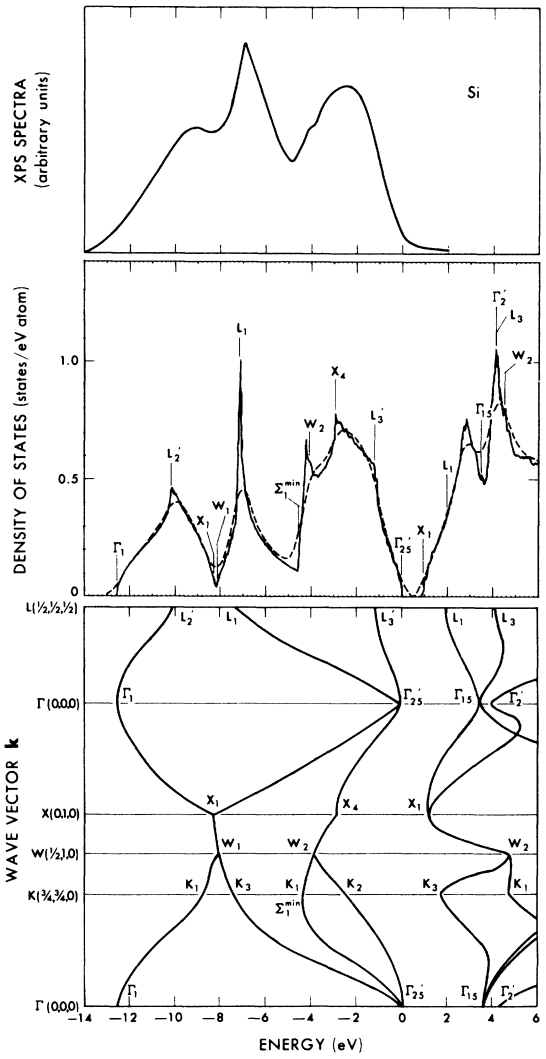

FIG. 1. X-ray photoemission spectra, density of states, and band structure for Si. The top figure shows the corrected experimental spectra from the XPS work of Refs. 1, 2, and 13. The middle figure is the EPM-calculated density of states. To facilitate comparison with experiment a broadened density of states is indicated by the dashed line. The bottom figure is the EPM-calculated band structure.

metric form factors $V^A(G)$ are zero.] The above series usually converges rapidly enough so that only three form factors are needed for each atom.

As a starting point for these calculations the CB form factors were used.[5] Adjustments were then made in these form factors to obtain a good fit to the experimentally determined density of states. The principal optical transitions at Γ, X, L, and Σ were constrained to remain near their original values.

One modification of the usual procedure used in EPM calculations was made. As is well known, the pseudopotential appearing in Eq. (1) is nonlocal. However, the local approach can be simply modified to take this fact into account in an approximate way. It has been noted[2,4] that the lowest-order correction to this inherent nonlocal behavior is to replace the free-electron mass in the Hamiltonian by an effective mass m^*. Such a procedure has been used before in EPM calculations especially when fits to orthogonalized-plane-wave results[6] are needed.

This approach is required here because the valence bands of interest span an energy range ~15 eV over which it was found that the pseudopotential could not be treated by purely local methods. Local approximations to the potential were sufficient for reflectivity fits since the transitions involved were direct, of low energy, and mainly between the top valence and bottom conduction bands. When indirect interband splittings were known, nonlocal adjustments were necessary.[7] This is similar to what we find for photoemission where the measured density of states gives us information about nondirect splittings.

Spin-orbit interactions were included for InSb, ZnSe, and CdTe. Here the spin-orbit splittings are comparable to the experimental resolution. The method of calculation used was that due to Weisz[8] as modified by Bloom and Bergstresser.[9] In this procedure two parameters are used to characterize the spin-orbit coupling.[10] The metallic spin-orbit parameter is varied until one obtains the experimentally known splittings, while the nonmetallic parameter is constrained to a fixed ratio between the two parameters. This ratio is equal to that of the ratio of the spin-orbit interaction for the free atoms as calculated by Herman and Skillman.[11] The resulting values for the metallic spin-orbit parameters for ZnSe, InSb and CdTe are 0.0006, 0.0019, and 0.0013, respectively.

Once the band structure has been obtained, the density of states $N(E)$ may be calculated from

$$N(E)=\frac{1}{NN_a}\sum_{\vec{K}}\sum_{n,\sigma}\delta(E-E_{n,\sigma}(\vec{K})), \tag{3}$$

where N is the number of primitive cells, N_a is the number of atoms in the primitive cell, and $N(E)$ is normalized to the number of states per atom. Equation (3) was evaluated by using the Gilat-Raubenheimer technique.[12] The energy derivatives required by this technique were obtained by using $\vec{k}\cdot\vec{p}$ perturbation theory. A grid of 308 points in the irreducible Brillouin zone was used in the calculation.

As in the case of analyzing optical reflectivity spectra, one can identify critical points in the density of states. These points determine the regions of the Brillouin zone responsible for the structure found in the density of states. By observing the relationship of critical-point locations in broadened and unbroadened density-of-states calculations, it is possible to obtain values for the actual positions of the critical points from experimental data.[2,3,13]

The resulting form factors, effective mass

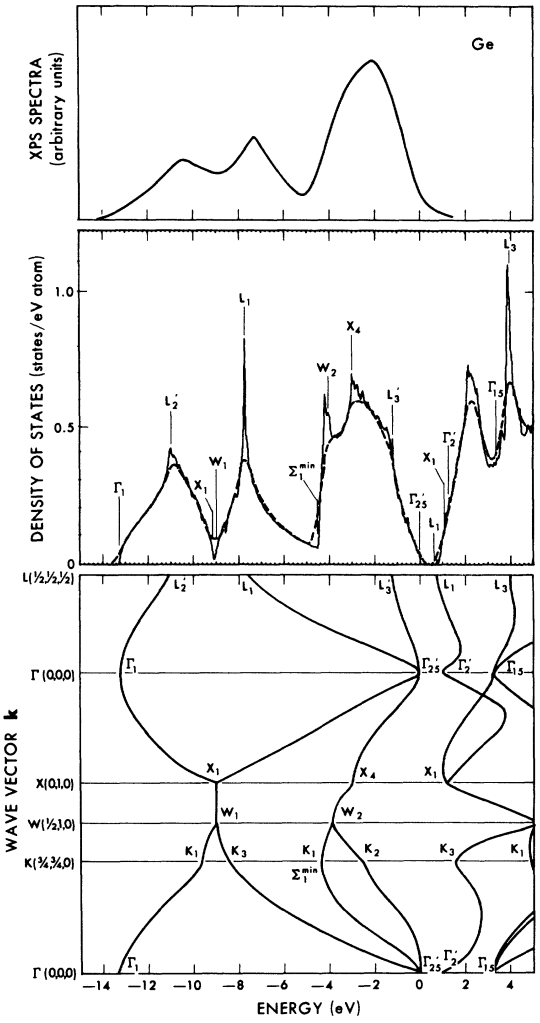

FIG. 2. X-ray photoemission spectra, density of states, and band structure of Ge. See Fig. 1.

TABLE III. Energies (in eV) of characteristic features in the valence band of Ge (measured relative to the top of the valence band).

	Theory		Experiment	
Ge	Old (Ref. 5)	New	UPS (Refs. 3, 14)	XPS (Refs. 1, 2, 13)
L_3	−1.1	−1.2	−1.1±0.2	•••
X_4	−2.4	−3.0	•••	−2.7±0.3
W_2	−3.3	−4.0	•••	−3.9±0.2
$\Sigma_1^{\min}$	−3.8	−4.4	−4.5±0.2	−4.5±0.3
L_1	−6.9	−7.8	−7.7±0.2	−7.4±0.2
W_1	−8.2	−9.1	•••	−8.7±0.3
L_2'	−9.9	−11.0	−10.6±0.3	−10.5±0.4
Γ_1	−12.0	−13.3	−12.6±0.3	−12.8±0.4

parameters, and lattice constants used in the calculations are listed in Table I.

III. RESULTS

In Figs. 1–7 the calculated densities of states are compared with the experimental results of XPS.[1,2,13] The band structures are also presented for each compound. In Tables II–VIII the resulting values for various characteristic features in the density of states are listed and compared with the results of previously calculated form factors from optical data.[5] (For these calculations the matrix size was larger than in the CB case, i.e., $E_1 = 9$ rather than the CB value $E_1 = 7$; this gives some slight shifts in the energies.) Tables II–VIII also contain the experimental results from both XPS[1,2,13] and UPS.[3,14] All energy positions are measured relative to the top of the valence band as shown in the figures.

When comparing the calculated density of states using a local pseudopotential (CB) with XPS and UPS data, it was found that several bands were in error by as much as 0.5–2.0 eV. The largest error is for the lowest-lying valence bands. Early workers recognized that the lower valence bands were not expected to be accurate since only interband transitions between the top valence and bottom conduction bands were used in the fitting procedure. As a result they did not publish the values or band-structure curves for these lower bands. We have computed these bands using the form factors given in the early papers, and we have extended the energy range in this way.

The addition of an effective mass parameter brings the calculated bands closer to experiment. This is not always the case for the lowest valence band, because our method is approximate and is designed to give the first band [especially near (0, 0, 0)] a low-energy value. A full nonlocal potential which accounts for d states in the core should work better, but it is a bit more complex. The effective mass approach does, however, remove all the major discrepancies for the higher bands. In particular, the $\Sigma_1^{\min}$ feature (which is

TABLE IV. Energies (in eV) of characteristic features in the valence band of GaAs (measured relative to the top of the valence band).

	Theory		Experiment	
GaAs	Old (Ref. 5)	New	UPS (Refs. 3, 14)	XPS (Refs. 1, 2, 13)
L_3	−0.9	−0.9	−0.8±0.2	−1.4±0.3
X_5	−2.2	−2.5	•••	−2.5±0.3
W_2	−2.6	−3.5	•••	−4.0±0.2
$\Sigma_1^{\min}$	−3.2	−3.9	−4.1±0.2	−4.4±0.2
W_1	−6.0	−6.6	•••	−6.6±0.2
X_3	−6.4	−6.8	−6.8±0.2	−7.1±0.2
X_1	−9.7	−11.4	−10.8±0.4	−10.7±0.3
Γ_1	−12.0	−13.8	−11.9±0.6	−13.8±0.4

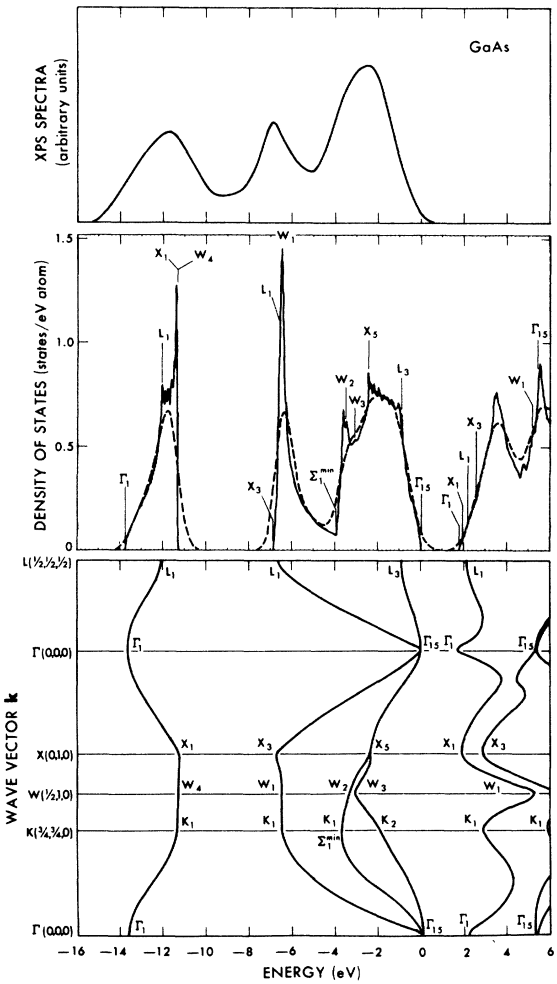

FIG. 3. X-ray photoemission spectra, density of states, and band structure of GaAs. See Fig. 1. Note that for zinc-blende crystals we have used L_1 for the two lowest bands at L to conform to the notation of other authors. Rigorously the labels should be L_1 and L_2.

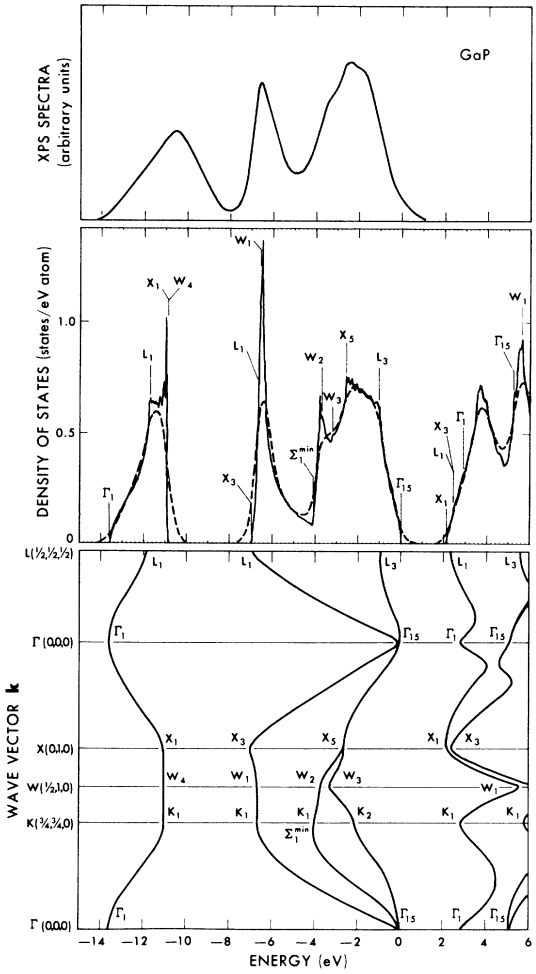

FIG. 4. X-ray photoemission spectra, density of states, and band structure of GaP. See Figs. 1 and 3.

sharp in UPS data) has been improved considerably.

The resulting densities of states are discussed below, compound by compound, and critical-point identifications are noted in parentheses where unambiguous determination is possible.

A. Silicon

In the case of Si (only) the original CB form factors were used, without an effective mass, to calculate the density of states. (See Fig. 1.) This was done because the resulting density of states agreed quite satisfactorily with the experimental results of both XPS and UPS (see Table II).

The threshold of the valence-band contributions to the density of states for Si is – 12.6 eV below the top of the valence band, and occurs at $\Gamma_1(M_0)$. The first peak at – 10.2 eV is from $L_2'(M_1)$. The contributions from the lowest band cease at – 8.15 eV at W_1 (M_3), while the minimum of the second band occurs at –8.3 eV at X_1 (M_0). The large peak at –7.2 eV comes from $L_1(M_2)$. Because of the rather sharp rise of the second valence band in the energy range from –7.2 to –4.5 eV, there is a rather sharp drop in the density of states from the L_1 peak. The onset of the third band occurs at –4.5 eV near K along Σ, thus the notation $\Sigma_1^{\min}$. The peak near – 4.1 eV arises from contributions near $\Sigma_1^{\min}$ and W_2 (M_1) at – 4.0 eV. The peak at – 2.8 eV is due to X_4 (M_2). Finally, the shoulder at – 1.1 eV is from L_3' (M_2).

B. Germanium

The valence-band contribution to the density of states for Ge begins at – 13.3 eV below the top of the valence band. (See Fig. 2 and Table III.) This point occurs at $\Gamma_1(M_0)$, while the peak at – 11.0 eV is due to L_2' (M_1). The contributions from the first band terminates at – 9.05 eV at W_1 (M_3), and the minimum of the second band occurs at – 9.15 eV at X_1 (M_0). The sharp peak at –7.8 eV arises from L_1 (M_2). Again there is a sharp drop in the density of states from – 7.8 to – 4.4 eV where the threshold of the third band occurs at $\Sigma_1^{\min}$. The peak near – 4.0 eV comes from the minimum along with contributions from W_2 (M_1). The peak at – 3.0 eV is due to X_4 (M_2). Finally the shoulder at – 1.2 eV comes from L_3' (M_2).

From Table III, one notes that the comparison with both UPS and XPS experimental results is quite satisfactory. A considerable improvement has been made from the CB results. Further, the discrepancy mentioned by Grobman and Eastman[3] for $\Sigma_1^{\min}$, namely, that the previous EPM calculation[5] and other band-structure calculations[15] give a value too close to the top of the valence band, has been removed. The calculated value of – 4.4 eV is quite close to the UPS and XPS value of – 4.5 eV. The agreement between theory and experiment would even be better if spin orbit were included. The agreement with experiment for the

TABLE V. Energies (in eV) of characteristic features in the valence band of GaP (measured relative to the top of the valence band).

	Theory		Experiment	
GaP	Old (Ref. 5)	New	UPS (Refs. 3, 14)	XPS (Refs. 1, 2, 13)
L_3	–0.9	–1.0	···	–1.4±0.3
X_5	–2.3	–2.5	···	–2.7±0.2
W_2	–3.2	–3.7	···	–3.6±0.2
$\Sigma_1^{\min}$	–3.8	–4.1	–4.2±0.3	–4.0±0.2
W_1	–5.4	–6.6	···	–6.5±0.2
X_3	–5.8	–6.9	–7.0±0.3	–6.9±0.2
X_1	–11.5	–10.9	···	–9.6±0.3
Γ_1	–13.0	–13.6	–12.0±0.6	–13.2±0.4

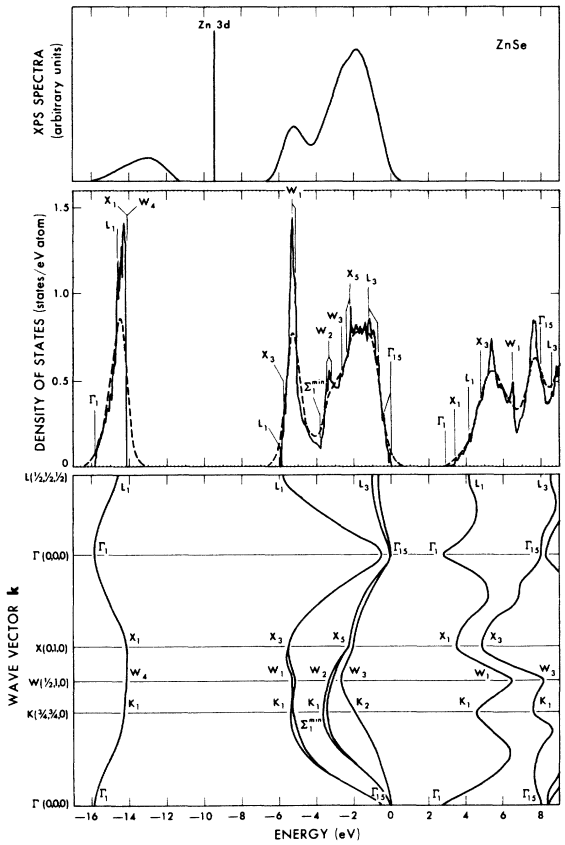

FIG. 5. X-ray photoemission spectra, density of states, and band structure of ZnSe. The Zn 3*d* states have been subtracted out, with the peak position indicated by the solid line. See Figs. 1 and 3.

L_2' and Γ_1 features has not improved significantly from the CB results.

C. Gallium Arsenide

The threshold of the density of states is at − 13.8 eV at Γ_1 (M_0). (See Fig. 3 and Table IV.) The shoulder at −12.1 eV arises from L_1 (M_1). The main peak at − 11.4 eV comes from the entire square face of the zone which turns out to be a surface of nearly constant energy (e.g., the energy change from X_1 to W_4 is less than 0.05 eV). Unlike the case of Ge there is a 4.5-eV gap between the two lowest valence bands. The gap extends from − 11.3 to − 6.8 eV and can be associated with the fact that the antisymmetric form factors, $V^A(G)$, are no longer zero as in the case of Ge or Si. The minimum of the second band occurs at X_3 (M_0). Contributing to the sharp rise, and to the large peak at − 6.5 eV are critical points at − 6.7 and − 6.6 eV arising from L_1 (M_1) and W_1 (M_1), respectively. Just as in the case of Ge, there is a sharp drop near the main peak; this drop continues until the minimum of the third valence band occurring at $\Sigma_1^{\min}$ at − 3.9 eV is reached. This, along with W_2 at − 3.5 eV, causes the sharp rise

TABLE VI. Energies (in eV) of characteristic features in the valence band of ZnSe (measured relative to the top of the valence band).

	Theory		Experiment	
ZnSe	Old (Ref. 5)	New	UPS (Refs. 3, 14)	XPS (Refs. 1, 2, 13)
L_3	−0.5	−0.9	···	−1.3±0.3
X_5	−1.5	−2.1	···	−2.1±0.3
W_2	−2.0	−3.3	···	−2.6±0.2
$\Sigma_1^{\min}$	−2.7	−3.8	−4.0±0.3	−3.4±0.4
W_1	−3.4	−5.3	···	−5.2±0.2
L_1	−3.8	−5.9	−5.7±0.3	−5.6±0.3
X_1	−13.2	−14.2	···	−12.5±0.4
Γ_1	−14.2	−15.8	···	−14.5±0.6

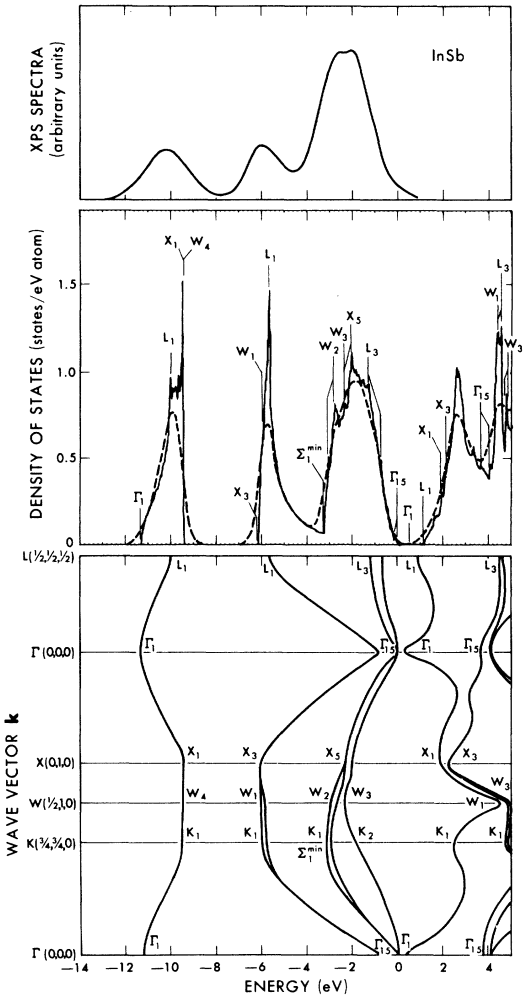

FIG. 6. X-ray photoemission spectra, density of states, and band structure of InSb. See Figs. 1 and 3.

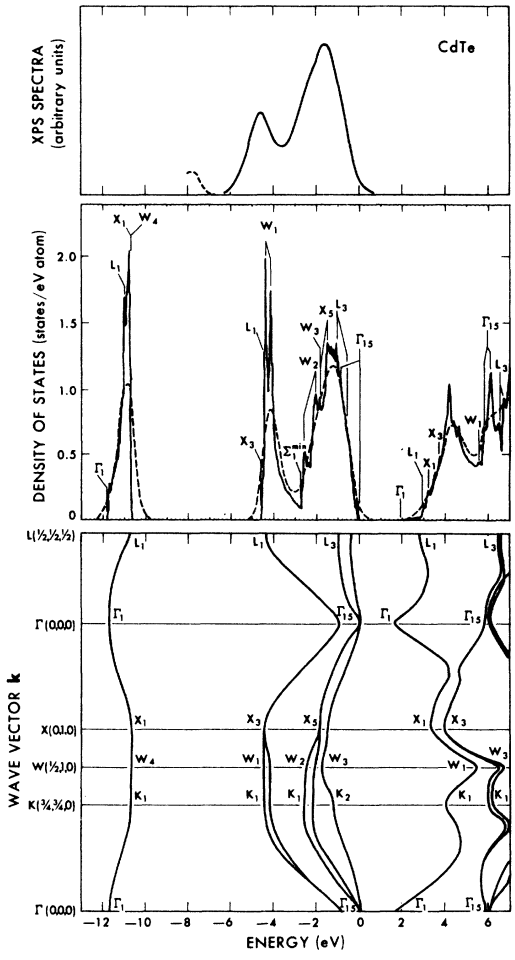

FIG. 7. X-ray photoemission spectra, density of states, and band structure of CdTe. See Figs. 1 and 3.

at the $\Sigma_1^{\min}$ edge. This fourth band has a minimum at W_3 (M_0) which leads to the gradual rise to the X_5 (M_2) peak at − 2.5 eV. The shoulder at − 0.9 eV is from L_3 (M_2).

Table IV shows that the agreement of the calculated energies with experiment has improved considerably from the CB results. The discrepancy noted by Grobman and Eastman[3] for $\Sigma_1^{\min}$ has again been removed and would be even smaller if spin-orbit effects were included.

TABLE VII. Energies (in eV) of the characteristic features in the valence band of InSb (measured relative to the top of the valence band).

	Theory		Experiment	
InSb	Old (Ref. 5)	New	UPS (Refs. 3, 14)	XPS (Refs. 1, 2, 13)
L_3	−0.6	−1.2	•••	−1.4±0.2
X_5	−1.4	−2.1	•••	−2.4±0.4
W_2	•••	−2.8	•••	−3.1±0.2
$\Sigma_1^{\min}$	−2.1	−3.2	−3.3±0.3	−3.4±0.2
L_1	−4.9	−5.7	•••	−5.9±0.2
X_3	−5.4	−6.2	−6.2±0.3	−6.4±0.2
X_1	−7.6	−9.5	−9.6±0.3	−9.5±0.2
Γ_1	−8.9	−11.3	−10.9±0.5	−11.7±0.3

TABLE VIII. Energies (in eV) of the characteristic features in the valence band of CdTe (measured relative to the top of the valence band).

	Theory		Experiment	
CdTe	Old (Ref. 5)	New	UPS (Refs. 3, 14)	XPS (Refs. 1, 2, 13)
L_3	−0.4	−1.0	−0.7±0.3	−0.9±0.3
X_5	−1.0	−1.5	•••	−1.8±0.2
W_2	−1.4	−2.0	•••	−2.2±0.3
$\Sigma_1^{\min}$	−2.0	−2.7	−2.9±0.3	−2.7±0.3
W_1	−2.6	−4.3	•••	−4.5±0.1
X_3	−2.9	−4.6	−4.8±0.2	−5.2±0.2
X_1	−12.5	−10.6	−8.8±0.3	•••
Γ_1	−12.9	−11.8	−10.8±0.6	•••

D. Gallium Phosphide

The calculated density of states for GaP is nearly identical to that of GaAs. (See Fig. 4 and Table V.) The threshold occurs at − 13.6 eV Γ_1 (M_0), while the shoulder at − 11.8 eV corresponds to L_1 (M_1). As in GaAs the square face of the Brillouin zone causes the huge peak at − 10.9 eV. There is a 4-eV gap which extends from − 10.9 to − 6.9 eV between the lowest valence band and the next higher band. The minimum of the second band is at X_3 (M_0), which occurs at − 6.9 eV. The sharp rise near the main peak at − 6.5 eV comes from L_1 (M_0) at − 6.7 eV and W_1 at − 6.6 eV. The contribution of the third band at $\Sigma_1^{\min}$ starting at − 4.1 eV causes the sharp rise in the density of states; W_2 (M_1) at − 3.7 eV also adds to the rise. The threshold of the fourth band occurs at W_3 (M_0) at − 3.0 eV and this starts the gradual rise to the X_5 (M_2) peak at − 2.5 eV. The shoulder at − 1.0 eV is from L_3 (M_2).

There is good agreement between experiment and the calculated values for the top three bands. There has been a considerable improvement over the CB results for the W_1 and X_3 states. For $\Sigma_1^{\min}$ the change was smaller. This is probably due to the fact that GaP is an indirect semiconductor and the indirect transitions were fitted roughly to the correct values by Cohen and Bergstresser when they considered the existing optical data.

E. Zinc Selenide

Since spin-orbit coupling was included in the following densities-of-states calculations, the degeneracy of the bands in certain directions can be removed. Hence, the bands will be labeled 1 through 8, with 1 being the lowest valence band

and 8 being the top valence band. To facilitate comparisons with Si, Ge, GaP, and GaAs the bands are labeled using non-spin-orbit notation. (See Fig. 5 and Table VI.)

The lowest two bands (1 and 2) are s like; thus spin-orbit interactions can be neglected. The minimum of the density of states occurs at Γ_1 (M_0) at − 15.8 eV. The shoulder at −14.6 eV is due to L_1 (M_2), while the large peak at − 14.2 eV is again due to the constant-energy surface of the square face of the Brillouin zone. The gap to the next higher band found in zinc blende extends from − 14.2 to − 5.9 eV. At − 5.9 eV, bands (3 and 4) start to contribute at L_1 (M_0). Interestingly enough, X_3 is not the minimum here as was the case in GaP or GaAs. Since L_1 is lower than X_3, the large peak at − 5.4 eV comes from X_3 (M_1) at − 5.8 eV and W_1 which is split by the spin-orbit interaction into two peaks: one at − 5.3 eV, the other at − 5.0 eV. The minimum of band 5 occurs at $\Sigma_1^{\min}$ at − 3.8 eV. The doublet peaks at − 3.4 and − 3.2 eV are caused by the splitting of bands (5 and 6) at W_2, and the sharp rise at − 2.7 eV is from the onset of bands (7 and 8) at W_3 (M_0). The large peak at − 2.1 eV is from bands (5 and 6) at X_5 (M_2), while the shoulder at − 0.9 eV is from bands (5 and 6) at L_3 (M_3). The spin-orbit splitting here causes another shoulder at − 0.7 eV from bands (7 and 8) at $L_3(M_3)$.

The agreement as indicated in Table VI is satisfactory except for the lowest band. Again there is marked improvement over the CB results.

F. Indium Antimonide

In InSb the spin-orbit coupling was included. (See Fig. 6 and Table VII.) The threshold for the lowest band occurs at − 11.3 eV at Γ_1 (M_0), while the shoulder occurring at − 10.0 eV is from L_1 (M_1). The sharp peak at − 9.5 eV comes from the square face of the Brillouin zone as in the other zinc-blende compounds. Again a gap appears between the two lowest valence bands. It begins at − 9.4 eV and terminates at X_3 (M_0) at − 6.2 eV. Unlike the other calculated densities of states, W_1 lies between X_3 and L_1. At W_1 spin-orbit interactions split bands 5 and 6 by about 0.2 eV. Both of these points occurring at − 6.0 and − 5.8 eV contribute to the peak at − 5.7 eV. L_1 (M_2) occurs at − 5.7 eV at the height of the peak. Band 5 has a threshold at − 3.2 eV at $\Sigma_1^{\min}$. The peaks at − 3.1 and − 2.8 eV are from the spin-orbit split bands at W_2 (bands 5 and 6). The small peak at − 2.4 eV is from bands (7 and 8) at W_3 (M_0) and X_5 (M_2) bands (5 and 6). The peak at − 2.1 eV is from bands (7 and 8) at X_5 (M_2), while the shoulder at − 1.2 eV is due to L_3 (M_3) from bands (5 and 6).

The comparisons with experimental results found in Table VII are very good. Even the lowest band agrees with the experimental results. It is, perhaps, noteworthy that the d states lie well below the lowest valence band. XPS data indicate the In $4d$ level lies about 17 eV below the top of the valence band.

G. Cadmium Telluride

Spin-orbit interactions were again included in the calculations for CdTe. (See Fig. 7 and Table VIII.) The threshold of the lowest band is at − 11.8 eV at Γ_1 (M_0). The two peaks in the lowest band at − 11.0 and − 10.6 eV are caused by L_1 (M_2) and by the nearly constant energy surface of the square face of the Brillouin zone, respectively. The gap between the lowest band and the next lowest band begins at − 10.6 eV and terminates at −4.6 eV at X_3 (M_0). The spin-orbit splitting between bands 3 and 4 at W_1 causes the doublet peaks at − 4.3 and − 4.0 eV. At − 4.4 eV, L_1 (M_1) adds to the height of the first peak. The minimum of band 5 again occurs at $\Sigma_1^{\min}$. This causes the sharp rise at − 2.7 eV. Spin-orbit splitting between bands 5 and 6 at W_2 causes the peaks at − 2.4 and − 2.0 eV. The peak at − 1.8 eV is due to the coincidenc of W_3 (M_0) from bands (7 and 8) and X_5 (M_2) from bands (5 and 6). The peak at − 1.5 eV is due to X_5 (M_2) from bands (7 and 8). Finally the shoulde at − 1.0 eV is due to bands (5 and 6) at L_3 (M_3).

The comparison with experiment is listed in Table VIII. The over-all agreement is satisfacton although the lowest band is in poor agreement with experiment.

IV. DISCUSSION OF RESULTS

One can observe some interesting trends by examining the isoelectric series of Ge, GaAs, and ZnSe. The most obvious change from Ge to GaAs is that a gap appears between the first two valence bands. As previously noted[2] this is due to the localization of electrons in the first band around the strong As ion,[16] and can be related to the antisymmetric from factors $V^A(G)$. This "antisymmetric gap" may also be related to the ionicity.[17] One notes that the gap nearly doubles in size from the 4.5 eV value in GaAs to 8.2 eV in ZnSe, which is more ionic.

Another trend observed in the calculated density of states is that the widths of the various peaks decrease as the compound becomes more ionic. For example, the width of the lowest band is 4.1 eV in Ge, 2.4 eV in GaAs, and 1.7 eV in ZnSe. The width of the top three bands also decreases. In Ge the width is 9.1 eV, in GaAs, 6.8 eV and in ZnSe, 6.0 eV.

The trends in going from InSb to CdTe follow the trends in going from GaAs to ZnSe. Namely, the antisymmetric gap for InSb is 3.3 eV, while the gap is 6.0 eV for CdTe. Finally, the width of the

lowest band for InSb and CdTe is 1.9 and 1.2 eV, respectively, and the top three bands also contract: 6.0 eV for InSb, and 4.6 eV for CdTe.

In summary, it has been demonstrated that the EPM, with the addition of an effective mass, can adequately reproduce the experimentally determined density of states for at least the top three valence bands. In addition, complete critical-point analysis has been given, and the experimental structure identified.

ACKNOWLEDGMENTS

We would like to thank D. A. Shirley, R. Pollak, L. Ley, S. Kowalczyk, W. D. Grobman, and D. E. Eastman for helpful discussions and for data before publication. Part of this work was done under the auspices of the U. S. Atomic Energy Commission.

---

*Supported in part by the National Science Foundation Grant No. GH 35688.

†National Science Foundation Predoctoral Fellowship.

[1]L. Ley, S. Kowalczyk, R. Pollak, and D. A. Shirley, Phys. Rev. Lett. **29**, 1088 (1972).

[2]R. Pollak, L. Ley, S. Kowalczyk, D. A. Shirley, J. D. Joannopoulos, D. J. Chadi, and M. L. Cohen, Phys. Rev. Lett. **29**, 1103 (1972).

[3]W. D. Grobman and D. E. Eastman, Phys. Rev. Lett. **29**, 1508 (1972)

[4]M. L. Cohen and V. Heine, Solid State Phys. **24**, 37 (1970).

[5]M. L. Cohen and T. K. Bergstresser, Phys. Rev. **141**, 789 (1966); referred to here as CB.

[6]F. Herman *et al.*, in *Proceedings of the International Conference of II-VI Semiconducting Compounds*, Brown University, 1967 (Benjamin, New York, 1967).

[7]C. Varea de Alvarez, J. P. Walter, M. L. Cohen, J. Stokes, and Yu. R. Shen, Phys. Rev. B **6**, 1412 (1972).

[8]G. Weisz, Phys. Rev. **149**, 504 (1966).

[9]S. Bloom and T. K. Bergstresser, Solid State Commun. **6**, 465 (1968).

[10]J. P. Walter, M. L. Cohen, Y. Petroff, and M. Balkanski, Phys. Rev. B **1**, 2661 (1970).

[11]F. Herman and S. Skillman, *Atomic Structure Calculations* (Prentice-Hall, Englewood Cliffs, N. J., 1963).

[12]G. Gilat and L. J. Raubenheimer, Phys. Rev. **144**, 390 (1966).

[13]L. Ley, R. Pollak, S. Kowalczyk, and D. Shirley (unpublished).

[14]W. D. Grobman and D. E. Eastman (unpublished).

[15]See, for example, D. J. Stukel, T. C. Collins, and R. N. Euwema, in *Proceedings of the Third International Materials Research Symposium*, Gaithersburg, Maryland, 1969, edited by L. H. Bennett, Nat. Bur. St. Special Publication No. 323 (U. S. GPO, Washington, D.C., 1971).

[16]J. P. Walter and M. L. Cohen, Phys. Rev. B **4**, 1877 (1971).

[17]W. D. Grobman, D. E. Eastman, and M. L. Cohen Phys. Lett. A **43**, 49 (1973).